Tunable distribution of silica nanoparticles in water-borne coatings via strawberry supracolloidal dispersions

Journal of Colloid and Interface Science 646 (2023) 185–197

Contents lists available at ScienceDirect

Journal of Colloid And Interface Science

journal homepage: www.elsevier.com/locate/jcis

Tunable distribution of silica nanoparticles in water-borne coatings via strawberry supracolloidal dispersions

Siyu Li [a], Leendert G.J. van der Ven [a], Anne B. Spoelstra [a,b], Remco Tuinier [a,c], A. Catarina C. Esteves [a,c,*]

[a] Laboratory of Physical Chemistry, Department of Chemical Engineering and Chemistry, Eindhoven University of Technology, P.O. Box 513, 5600 MB Eindhoven, The Netherlands
[b] Center for Multiscale Electron Microscopy, Department of Chemical Engineering and Chemistry, Eindhoven University of Technology, P.O. Box 513, 5600 MB Eindhoven, The Netherlands
[c] Institute for Complex Molecular Systems (ICMS), Eindhoven University of Technology, P.O. Box 513, 5600 MB Eindhoven, The Netherlands

GRAPHICAL ABSTRACT

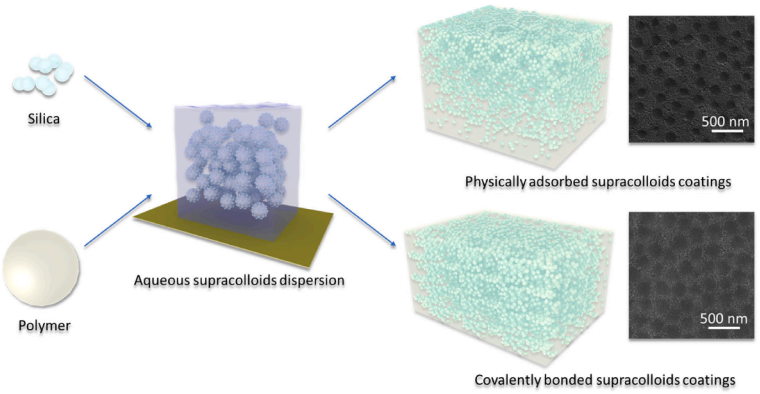

ARTICLE INFO

Keywords:
Waterborne coatings
Supracolloids
Silica nanostructures
Stratification
Dispersions

ABSTRACT

Hypothesis: Water-borne coatings are rapidly expanding as sustainable alternatives to organic solvent-borne systems. Inorganic colloids are often added to aqueous polymer dispersions to enhance the performance of water-borne coatings. However, these bimodal dispersions have many interfaces which can result in unstable colloids and undesirable phase separation. The covalent bonding between individual colloids, on a polymer-inorganic core-corona supracolloidal assembly, could reduce or suppress instability and phase separation during drying of coatings, advancing its mechanical and optical properties.
Methods: Aqueous polymer-silica supracolloids with a core-corona strawberry configuration were used to precisely control the silica nanoparticles distribution within the coating. The interaction between polymer and silica particles was fine-tuned to obtain covalently bound or physically adsorbed supracolloids. Coatings were prepared

* Corresponding author at: Laboratory of Physical Chemistry, Department of Chemical Engineering and Chemistry, Eindhoven University of Technology, P.O. Box 513, 5600 MB Eindhoven, The Netherlands.
E-mail address: a.c.c.esteves@tue.nl (A.C.C. Esteves).

https://doi.org/10.1016/j.jcis.2023.04.154
Received 22 March 2023; Received in revised form 21 April 2023; Accepted 27 April 2023
Available online 5 May 2023

by drying the supracolloidal dispersions at room temperature, and their morphology and mechanical properties were interconnected.

Findings: Covalently bound supracolloids provided transparent coatings with a homogeneous 3D percolating silica nanonetwork. Supracolloids having physical adsorption only, resulted in coatings with a stratified silica layer at interfaces. The well-arranged silica nanonetworks strongly improve the storage moduli and water resistance of the coatings. These supracolloidal dispersions offer a new paradigm for preparing water-borne coatings with enhanced mechanical properties and other functionalities, like structural color.

1. Introduction

Conventional (organic) solvent dispersions, inks, and coatings formulations have been used for many decades for the most varied purposes. These dispersions often contain organically modified nanofillers which can be well-dispersed in the organic solution. Once the dispersions are applied on a substrate and dried out, a solid composite film is formed, where the distribution of the insoluble nanofillers plays an important role in the coatings and films properties [1–6] namely on the reinforcement of the mechanical properties, such as hardness and scratch resistance, [7,8] the improvement of conductivity, [9,10] or the enhancement of optical properties [7,11].

With rising environmental and health concerns, liquid formulations are increasingly required to be more sustainable and use water as dispersing medium. Aqueous dispersions of colloidal polymer particles are the typical liquid formulations (paints) used for water-borne coatings and inks [12,13]. Polymers used in these dispersions commonly have low glass transition temperature (T_g) so that once the dispersion is cast on a substrate and the water starts evaporating, the polymer chains have sufficient mobility to diffuse across polymer particles and form a cohesive solid film. Inorganic nanofillers are also often incorporated in these aqueous polymer dispersions to obtain colloidal composite mixtures with enhanced properties and plentiful applications on inks, drug delivery systems, food & cosmetics, and in general paints [14–17]. The distribution of inorganic nanoparticles in the solidified layer and the formation of a homogenous nanocomposite is highly relevant to the mechanical, thermal and chemical resistance performance of water-borne polymer coatings.

Several preparation methods, such as Ramsden-Pickering emulsion polymerization and *in situ* polymerization [3,5,18–22] have been reported to fabricate nanocomposite supracolloidal particles which are stable in aqueous dispersions. These dispersions are then applied on substrates with the main aim of obtaining polymer coatings with homogeneously distributed inorganic nanoparticles (fillers). The mentioned preparation methods are very advantageous, mainly because the solid inorganic nanoparticles act as stabilizers and are naturally positioned/distributed at the surface of the polymer colloids. However, Pickering emulsifiers (inorganic nanoparticles) can also partially hinder the molecular diffusion of the polymer chains between polymer particles resulting in high(er) film formation temperature [23,24]. González-Matheus *et al.* [23] reported that water-borne films obtained from large Pickering supracolloids required higher film formation temperature compared to small(er) Pickering systems, for supracolloids with the same silica weight fraction in the corona. On the other hand, *in situ* polymerization [20,25] can possibly originate a discontinuous or aggregated inorganic phase in the nanocomposite. The aggregation number of the nanofillers, *i.e.,* effective filler-filler interactions, as well as the fillers networks eventually formed within the coatings, are extremely important for the mechanical properties of nanocomposite materials [26,27]. Furthermore, according to the classic film formation mechanism from a polymer (latex) dispersion, molecular diffusion of the polymer chains throughout the particle's boundaries (*i.e.*, coalescence) is key to obtain a stable and homogenous solidified layer [28].

One alternative route to prepare supracolloidal particles is the straightforward mixing of pre-prepared colloids of different types in an aqueous medium to obtain stable colloidal dispersions, often mediated by the presence of stabilizers and surfactants. One advantage of this route is that the polymer-filler weight ratio can be easily varied. Nevertheless, upon application and drying of these dispersions, multiple colloidal and molecular interactions play a role in the aqueous medium. These interactions influence major physical properties, such as surface tension and osmotic pressure, [29] and can trigger several (often undesired) phenomena such as aggregation, [30] deposition, [31] and stratification [31–34]. The large majority of water-borne coatings contain polymer colloids with diameters between 50 and 1000 nm, on a high solid content formulation and smaller inorganic nanoparticles. Since colloids of different sizes have different mobility in the wet/drying film, some of the particles tend to be trapped at the air-coatings interface due to the large Peclet number. Hence, the stratification into a one-size colloid domain has been often observed at the air interface [31–34]. Such phenomena influence the final structure and composition of coatings and applied films. Additionally, the presence of free-moving stabilizers and surfactants is one major concern in these so-called "heterocoagulated" systems, as the small molecules play a key role in the stability of the particles in the dispersion. Furthermore, they strongly influence assembly processes occurring in the aqueous medium and have an impact on the nanocomposite coatings morphology and bulk structure. Their interaction with fillers can result in different distributions of the fillers in a coating, which ultimately impacts its properties [35]. Martín-Fabiani *et al.*[36] and Limousin *et al.*[37] compared colloidal nanocomposites obtained by different preparation approaches discussed above. By blending, a discontinuous inorganic network was obtained in the polymer matrix, and by Pickering emulsion polymerization with the same chemical composition more homogenous coatings were made. Both studies concluded that the presence of a continuous nanofillers network effectively improves the moduli of the nanocomposite films. For other similar Ramsden-Pickering systems, the final properties of films were unfortunately only seldom investigated [23,38,39]. In general, it has been reported that the presence of 3D percolating networks of both filler and polymer phases is a prerequisite for the good performance of water-borne coatings, including outstanding mechanical properties.[40,41].

The methods described have been applied in the preparation of polymer-silica colloidal systems [3,5,18–22,42,43] which are used on water-borne polymer coatings, with the main objective to improve the coatings mechanical and thermal performance. Typically, colloidal supracolloids with core-corona morphology can be obtained with particles of varying sizes and size ratios. For coating applications, the most relevant nanocomposites consist of spherical polymer particles, and the corona can be a layer of individual silica nanoparticles with different configuration, *e.g.*, raspberry (with polymer-cores fully covered by the corona-inorganic nanoparticles)[18,19] or strawberry (partial corona surface coverage)[44]. In Pickering nanocomposite dispersions, the high-volume fraction of fillers often leads to formation of raspberry supracolloids. [18,19,45] The raspberry configuration can partially hinder the molecular diffusion of the polymer chains throughout the particle's boundaries,[28] resulting in high(er) film formation temperature,[23,24] or less good optical and mechanical properties. [18,19,29,30] On the contrary, the strawberry configuration[44] could make a good compromise between reasonable film formation properties (*i.e.*, sufficient mobility for polymer chains interdiffusion), low aggregation of the nanofillers, and the build-up of continuous 3D

nanonetworks.

In our previous work, we studied the assembly conditions to prepare stable core-corona polymer-silica supracolloidal particles with strawberry configuration, in aqueous dispersions.[44] By tunning the hydrophobic and electrostatic interactions between the colloids, supraparticles with controlled corona surface coverage, and variable core-corona mass ratio were prepared. Furthermore, if the strawberry configuration is stable and retained during application of these dispersions on a surface, drying and film formation steps, coatings with an overall homogeneous distribution of the silica nanoparticles are to be expected, with a high potential to form continuous 3D networks throughout the solidified layer.

In this work, we prepared water-borne coatings from concentrated aqueous dispersions containing polymer-silica core-corona supracolloids, with a strawberry configuration [44]. The distribution of the silica nanoparticles was well-controlled throughout the coating layer, by tuning the interactions between the polymer and silica nanoparticles in the assemblies. Two types of aqueous supracolloidal dispersions were used, where the assemblies were formed by physical adsorption only (mediated by a PEO-based surfactant, Triton X-405) or through covalent interactions between the particles (using thiol/disulfide chemical bonds). The supracolloidal dispersions were cast and dried in air and at room temperature. The supraparticles and coatings morphology were characterized by electron microscopy (SEM and cryo-TEM). Their chemical composition was investigated by Energy-Dispersive X-Ray Spectroscopy (EDX) and Attenuated Total Reflectance-Fourier Transform Infrared Spectroscopy (ATR-FTIR). We discuss the distribution of the silica nanoparticles and the resulting inner structure of the nanocomposite films, obtained from the different supracolloidal dispersions. The mechanical performance and water-uptake properties of the supracolloidal coatings were evaluated and are related to the surface and bulk morphology (nanonetworks or stratified silica-rich layers) obtained from the different supracolloidal dispersions.

2. Materials and methods

2.1. Materials

Butyl acrylate (99%, BA), methyl methacrylate (99%, MMA), and ethylene glycol dicyclopentenyl ether methacrylate (90%, DCPMA) were purchased from Sigma-Aldrich and purified via a basic alumina column (Honeywell, Brackman I) to remove inhibitors before polymerization. 2,2′-(Ethylenedioxy)diethanethiol (95%, EDT), 2-hydroxy-4′-(2-hydroxyethoxy)-2-methylpropiophenone (98%, HMPP), 2-amino-2-methyl-1,3-propanediol (99%, AMPD), citric acid (99%), poly (ethylene glycol) methyl ether methacrylate (PEGMA) solution (Mn ~ 2000 g/mol, 50 wt%), Triton X-405 solution (Mn ~ 1967 g/mol, 70 wt %), and Zeolite 13x were obtained from Sigma-Aldrich and used as received. The initiator 2,2′-azobis[2-(2-imidazolin-2-yl) propane] dihydrochloride (98%, AIBA) was used as received from Acros Organics. Levasil® silica aqueous colloidal dispersion (40 wt%, thiol functionalized) was kindly provided by Nouryon (Sweden), and further purified by dialysis or diafiltration as described in Supplementary Information (SI). The AMPD-citric acid aqueous solution was used as a buffer to adjust the pH and dilute the polymer and silica dispersions. For all experiments, deionized (DI) water (pH 6.5) filtered by an Elix® Reference water purification system was used.

2.2. Synthesis of thiol functionalized poly(butyl acrylate-co-methyl methacrylate) (EDT-G2.4) particles

The polymerization procedure of the DCPMA functionalized poly(BA-MMA) particles (G2.4) was performed as follows: The polymerization was carried out in a four-neck jacked flat-bottom reactor equipped with a reflux condenser, stainless steel stirrer with a half-moon shape, nitrogen gas inlet and dosing pump inlet. For the *seeds-emulsion* formation step 0.96 g butyl acrylate (BA), 0.96 g methyl methacrylate (MMA), 0.10 g Triton X-405 solution and 50 g deionized water were added into the flask and de-aired by bubbling with nitrogen for 30 min. The stirring speed was kept at 200 rpm and when the temperature reached 60 °C, 2.0 g of a 6.5 wt% aqueous initiator solution (AIBA) was added into the reactor. The polymerization proceeded for 30 min. Meanwhile, a *pre-emulsion* was prepared following the formulation shown in Table 1 and bubbled with nitrogen for 30 min. Subsequently, the *pre-emulsion* was fed into the glass reactor containing the *seeds-emulsion*, via a dosing pump along 150 min. 2 g of a 4.5 wt% AIBA aqueous solution was simultaneously added dropwise into the glass reactor when the *pre-emulsion* feeding started, along approximately 5 min. Finally, a *shell-emulsion* with 3 g BA, 1 g MMA, 2.2 g DCPMA, 0.2 g Triton and 4 mL of DI water previously bubbled with nitrogen, was fed into the glass reactor along 20 min. After all the step-emulsions have been added to the reactor, the polymerization continued for 90 min at 60 °C, after which it was quenched by exposing it to air. The polymer dispersions were saved in the fridge at 2 °C and used without further purification.

The thiol-group functionalization of the poly(BA-MMA-DCPMA) particles was performed as follows: 5 g of poly(BA-MMA) particles dispersion (33.6 wt%), 49.2 μL EDT and 100 μL HMPP aqueous solution (0.4 wt%) were added in a 20 mL glass vial with a magnetic stirrer. The glass vial was placed in a sealed photo-reactor chamber equipped with a nitrogen gas flow, a stirring plate and a S1000 OmniCure Mercury spot UV curing lamp (320–500 nm) with EXFO fiber light guides. The mixed dispersion was stirred at 1600 rpm and irradiated at 23 mW/cm^2 for 30 min. After the reaction, the vial was sealed under nitrogen atmosphere to prevent further oxidation of the thiol groups grafted on polymer particles surface, and subsequently used for the strawberry supracolloids assembly.

2.3. Assembly and thiol/disulfide exchange of the strawberry supracolloids: Covalently binding.

The assembly condition of strawberry supracolloids was illustrated in the previous study.[44] A typical preparation procedure of 12 wt% PA-G-Si.25/CB-G-Si.25 dispersion is described as follows: 2 mL 31.6 wt% G2.4/EDT-G2.4 polymer dispersion, adjusted pH 9.5 with 0.5 M AMPD solution, 1.7 mL 12.6 wt% silica dispersion (pH 9.5, diafiltration purified) were infused into a 20 mL sealed glass vial with 3.5 mL AMPD-citric acid buffer solution (30 mM) and the dispersion was stirred at 400 rpm. After 100 min, the infusion finished and the glass vial was sealed and stirred at room temperature to equilibrate for 10 days. The volume of silica suspension and buffer solution was adjusted by the silica solid content. The DCPMA functionalized poly(BA-MMA) polymer

Table 1
Characteristics of the polymer and silica nanoparticles used to prepare the supracolloidal dispersions: hydrodynamic diameter ($\bar{d}_H$), zeta potential (ζ) and concentration (C) of PEO in the initial polymer dispersions, and TEM diameter ($\bar{d}_{TEM}$), zeta potential (ζ), and thiol grafting density ($\sigma_{S\text{-}H}$) of silica nanoparticles.

Polymer core	$C_{PEGMA\text{-}PEO}$[&] (wt%)	$C_{Triton\text{-}PEO}$[&] (wt%)	$C_{Total\ PEO}$[&] (wt%)	C_{EDT}[&] (wt%)	$\bar{d}_H$(nm)[#]	ζ (mV)[#]
G2.4	2.4	2.2	4.6	–	269 ± 8	−16.9 ± 1.4
EDT-G2.4	2.4	2.2	4.6	3.3	269 ± 4	−20.9 ± 2.8
T4.6	–	4.6	4.6	–	232 ± 4	−24.4 ± 2.6
Silica	$\bar{d}_{TEM}$(nm)[^]	ζ (mV) [#]			$\sigma_{S\text{-}H}$ (mmol/g)[*]	
Si	27 ± 7	−57.4 ± 1			0.03	
HSi	33 ± 5	−55.6 ± 10			0.18	

[&] Over polymer core solid mass.
[#] Measured in pH 9.5 (10 mM AMPD-Citric acid) buffer.
[^] Average diameter estimated from 100 particles in Cryo-TEM images.
[*] Titration results using a dialyzed silica dispersion.

dispersion was assembled under the same condition to prepare physically adsorbed strawberry supracolloids.

The strawberry supracolloids fixation of silica on polymer particles was examined by adjusting pH to 11.5 with 1 M sodium hydroxyl solution. The dispersion state of the CB-G-Si.20 and PA-G-Si.20 supracolloids at pH 9.5 and 11.5 was investigated with Cryo-TEM. An aliquot from the dispersions with 12 wt% supracolloids, was taken at different assembly time points (within 30 days) and placed in a glass vial which was magnetically stirred for 1 min at 400 rpm. Cryo-TEM samples were prepared by depositing 3 μL of these dispersions on a 200 mesh Cu grid with Quantifoil® R2/2 100 holey carbon films (Quantifoil Micro Tools GmbH). All TEM grids were previously surface plasma treated for 40 s by a Cressington 208 carbon coater. Subsequently, samples were vitrified in liquid ethane using a vitrification robot (Vitrobot Mark IV, Thermo Fisher Scientific). Cryo-TEM samples were imaged in low-dose bright-field TEM mode using the TU/e cryo-TITAN electron microscope (Thermo Fisher Scientific, USA) which was operated at 300 kV, equipped with a field emission gun (FEG), a post-column Gatan Energy Filter (GIF, model 2002, Gatan, USA) and a post GIF 2 k × 2 k CCD camera (model 794, Gatan, USA).

2.4. Average particle diameter and zeta potential measurements

The hydrodynamic diameter of the individual particles and the supracolloids was measured by Dynamic Light Scattering (DLS) using an Anton Paar Litesizer 500 equipment, at 20 ℃. The dispersions were diluted with a pH 9.5 buffer solution (10 Mm AMPD-citric acid), with different buffer concentrations used for the assembly conditions, to 0.05 wt% and measured five times at a backscattering angle of 175°. Zeta potential values were obtained from the five measurements as well, with the Hueckel approximation. The errors given in Table 1 are the standard deviation of five repeated measurements.

2.5. Free-standing supracolloidal coatings preparation

The 12 wt% strawberry supracolloid dispersions were casted as polymer films on Teflon substrates with a 1 mm barrier a gap applicator and a 250 μm gap and dried in a glass curing box with a stable airflow at ambient temperature (22 ± 2 ℃) and 5 ± 2% humidity conditions for 6 h. The films were easily peeled from the substrate by hand and had a thickness of ≈ 80–120 μm, as measured by a digital micrometer (54–815 series, Fowler Xtra-value).

2.6. Silica nanoparticles distribution in supracolloidal coatings

The different chemical composition of the interface of nanocomposite film was determined by ATR-FTIR spectroscopy. The spectroscopy was performed on a Varian 670IR FT-IR spectrometer with a DTGS detector, collecting an average of 32 scans in the frequency range from 600 to 4000 cm^{-1}. For every free-stand film sample, both air-film and substrate-film interface were measured three times, and the average spectrum of three measurements was provided.

For SEM imaging of the cross-section of supracolloidal films before and after calcination, a piece of the free-stand films was frozen in liquid nitrogen, and a clear fracture was obtained by breaking the films at the liquid nitrogen temperature. The film was placed on a silicon wafer fixed to an SEM stub. Before imaging, a sputter-coated platinum layer was applied by using a Quorum Q150T Plus–Turbo molecular pumped sputter coater at 40 mV for 20 s. SEM imaging was conducted using dual-beam SEM Quanta 3D FEG (Thermo Fisher Scientific, USA), at an acceleration voltage of 5 KV. The probe current of all images is around 12 pA.

Energy-Dispersive X-Ray spectroscopy (EDX) mapping measurements were performed at an accelerating voltage of 10 kV using Phenom proX SEM (Thermo Fisher Scientific, USA). To avoid the different electron interaction volumes due to the inhomogeneity of two types of coatings, the total silica atomic concentration of one whole mapping area (~8 × 8 μm^2) was used, where the used relative depth was determined by the center of one mapping area. The average value of three mapping areas was used for each depth and the total interaction volume of all mapping areas was approximately the same. The interaction volume difference of silica and polymer can be negligible due to the average concentration of atoms in a large area used.

The ULACM method modified from the low-angle microtoming method reported by Hinder *et al.*[46] was used. Free-stand supracolloidal films were cut to a size of approximately 2 mm × 4 mm and attached to an epoxy block. Due to the cryogenic conditions, a cryo-glue was used between the films and the epoxy block instead of double-sided tape. The cryo-sectioning was performed using a 4 mm trimming knife (Diatome©) and operating at −20 °C (Leica UC7/FC7 cryo-microtome). The supracolloidal films were trimmed from the air-coating interface to the substrate-coating interface at an ultra-low angle against the epoxy block surface, which resulted in a full cross-section of about 2 mm × 3 mm over the full thickness (~100 μm). The trimmed specimens were soaked in DI water for 30 mins to remove the cryo-glue. After washing, the specimens were transferred to a Si wafer substrate and dried in ambient conditions after which they were ready for the slide-on ATR-FTIR measurement. The slide-on ATR FTIR microscope measurements were performed with the same Varian 670IR FT-IR spectrometer with a slide-on Si crystal. The position of the Si crystal was aligned with optical lenses of the IR microscope.

2.7. Dynamic mechanical thermal analysis of free-stand films

The films were put in an aging box at 70 ℃ with stable N_2 flow for 48 h to obtain a stable film for dynamic mechanical thermal analysis (DMTA) and water vapor adsorption measurements. The storage modulus and loss modulus of PA-G2.4-Si.25 coating after annealing were comparable with the moduli of the same coating aged in ambient conditions for 10 months in Fig. S7.

Temperature sweeps of storage modulus, loss modulus, and loss factor were determined by a rheometer (Physica MCR 301, Anton Paar) in a parallel configuration equipped with an H-ETD400 temperature control device, using a parallel-plate geometry of 7.946 mm. The measurements were conducted by the application of a constant normal force of 0.25 N to the film, with an angular frequency of 1 rad/s and a strain of 0.05%. The strains were chosen in the linear elastic region of supracolloidal films.

For DMTA with film clamper, the oscillation force is applied to the cross-section of coatings homogenously. When the temperature was above 50 ℃, the G2.4 sample broke, and the measurement automatically stopped. In the parallel-plate measurement, the oscillation distortion was first applied to the top surface of the coatings so that the creep behavior of different densities of the silica network was also reflected in the measurement. Parallel-plate rheology can measure the free-stand G2.4 coatings up to 90 ℃.

Before each measurement, the films were relaxed under 0.25 N axial force for 3 min at 22 ± 0.5 ℃ to reach an optimal contact between measurement plates and sample. Then, an increasing temperature profile was applied in which the temperature was increased from 22 ℃ to 90 ℃ for 140 min and 840 data points were obtained with an interval of 10 s. Three specimens/measurements were conducted for each coating sample, and those three specimens were prepared in different batches with the same formulation. The average results of three measurements were further averaged for every five points to reduce the noise caused by the limited resolution of the rheometer.

2.8. Water vapor uptake and diffusion

The WVU and water diffusion D_{water} across the film was determined using dynamic vapor sorption (DVS) (DVS resolution, Surface Measurement Systems). DVS is a gravimetric sorption technique that

measures how quickly and how much of a particular solvent, is absorbed by a sample by the weighing mechanism of an ultra-sensitive recording microbalance in which the sample and reference pans were enclosed in a humidity and temperature-controlled chamber. For WVU, the film was pre-dried at 0 % RH for 100 mins. Then, every 10% humidity step was taken from 0 to 80% humidity. Above 80% RH, the step increase was of 5% up to 95% RH. The end of each step was determined by dm/dt smaller than 0.001 mg/min. The diffusion coefficient of water D in films was calculated by the diffusion equation of thin film employed by Crank and Park [47,48],

$$\frac{M_t}{M_\infty} = \frac{4}{L}\sqrt{\frac{D_{water}t}{\pi}} \quad (4)$$

where M_t is the mass of adsorbed vapor at time t, M_∞ is the mass of adsorbed vapor at thermodynamic equilibrium, and L is the thickness of the films. L was measured two times and the average values of two measurements were used. One example of a fitted diffusion coefficient of water is available in SI. The WVU of the washed film was measured with the same protocol on the films which were previously soaked in DI water for two days and washed twice with DI water afterward. The films were dried in ambient conditions for at least 6 h. The supracolloidal coatings lost less than 2 % of the total weight after washing which is less than the total weight of the mass fraction of Triton surfactant.

3. Results and discussions

3.1. From colloidal dispersions to structured supracolloidal coatings

3.1.1. Preparation of supracolloids assemblies and coatings

Water-borne coatings were prepared from different types of aqueous dispersions of polymer-silica supracolloids. Previously, we reported the assembly of polymer-silica core-corona supracolloidal particles in aqueous dispersions [44]. We demonstrated that the silica mass fraction of the supracolloidal particles can be easily tuned to obtain dense 12 wt % aqueous dispersions by using a 30 mM pH 9.5 buffer solution, while the fraction of free silica nanoparticles in the dispersion remains negligible.

In this work, we use these concentrated supracolloids aqueous dispersions to prepare water-borne coatings by casting on Teflon substrates and drying at room temperature. The hydrodynamic diameter and shear-rate dependent viscosity profile of the 12 wt% supracolloidal dispersions prepared are provided in Table 1 and Supporting Information (SI), respectively. The corona of the strawberry supracolloids consists of silica nanoparticles (with hydrodynamic diameter $\overline{d}_H \approx$ 30 nm) functionalized with thiol (S-H) groups which were afterward oxidized to disulfides (-S-S-), see Scheme 1A. The thiol functionalization, purification, and post thiol-oxidation to disulfides of the silica nanoparticles are described in Methods and SI. The silica nanoparticles were denoted as "Si" (for low-) and "HSi" (for high-), according to the thiol/disulfide grafting density, see Table 1. The disulfide groups were subsequently used to covalently bind the silica nanoparticles to the polymer cores during the assembly process via thiol/disulfide bonds reshuffling, resulting in covalently bound strawberry supracolloids, see Scheme 1B. These particles further facilitate the crosslinking of the coating during film formation, see Scheme 1C.

The polymer core of the prepared supracolloids was obtained by emulsion polymerization using equiponderant quantities of methyl methacrylate (MMA) and butyl acrylate (BA). The particle diameter was primarily controlled by using Triton X-405 (a polyethylene oxide (PEO) based stabilizer) used in the seeding step of the semi-continuous emulsion polymerization. For some of the polymer particles, a small amount of the reactive polyethylene glycol methacrylate (PEGMA) co-monomer was also copolymerized to modify the surface of the polymer particles with PEO grafted chains. Hence, two types of polymer particles containing a similar overall mass fraction of PEO were prepared, with or without grafted chains, named as G2.4 and T4.6 respectively, where the number indicates the weight fraction of PEO from PEGMA or Triton stabilizer only, respectively, see Table 1. A fourth comonomer ethylene glycol dicyclopentenyl ether methacrylate (DCPMA) was added in the last step of the semi-continuous emulsion polymerization to introduce vinyl group functionalities at the polymer surface, which can undergo thiol/ene reactions. These vinyl groups were converted afterward into thiol/disulfide groups (Scheme 1A), by a pre-reaction with 2,2′-(ethylenedioxy)diethanethiol (EDT), which also acts as a crosslinker during the film formation. The thiol/ene reaction was carried out under UV irradiation. The characterization of this photoreaction and its efficiency is provided in Table S3. After thiol functionalization with EDT, the polymer particles (in Scheme 1A) were named as EDT-G2.4.

Nanocomposite/polymer coatings were prepared from aqueous dispersions combining the different individual particles listed in Table 2. The nomenclature of the coatings relates to the type of dispersions used and indicates: the type of interactions between the silica and polymer particles (CB-covalently bonded or PA-physically adsorbed), the type of PEO chains present (G-Grafted via PEGMA and *T*-Triton only), the silica surface functional density (HSi (high) and Si (low), Table 1), and the mass fraction of silica nanoparticles over total solid mass initially added to the dispersion (varying from 15 to 25 wt%). For example, CB-G-Si.20 indicates dispersions or coatings from supracolloids with silica

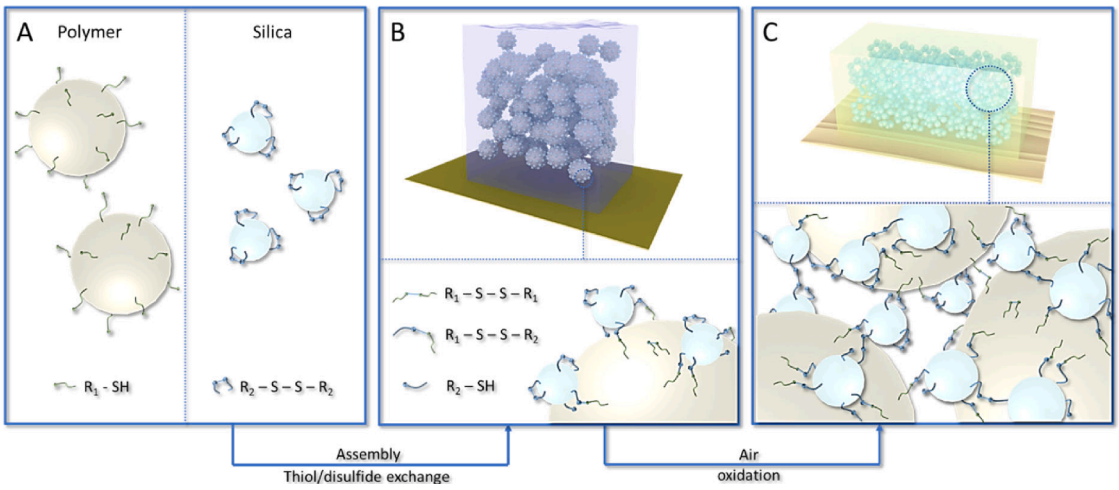

Scheme 1. Schematic of the particles surface modification (A) and thiol/disulfide bonds reshuffling that led to the formation of strawberry supraparticles in the dispersion (B). Crosslinked films form upon air drying and oxidation of the thiol/disulfide bonds (C).

Table 2
Coatings prepared from supracolloidal dispersions. Nomenclature according to the type of interaction between silica and polymer particles (CB-covalently bonded or PA-physically adsorbed), silica surface functional density (H-high, see Table 1), PEO chains type present in the dispersion (G-Grafted via PEGMA and *T*-Physically adsorbed Triton). The mass fractions and volume fractions (ϕ_{Si}) of silica nanoparticles in the supracolloidal coatings (Si.xx). All dispersions were used with an overall of 12 wt% supracolloids in the aqueous dispersions.

Supracolloidal coatings	C_{Si} (wt%) [#]	ϕ_{Si}
CB-G-Si	15	0.075
	20	0.10
	25	0.125
CB-G-HSi	20	0.10
PA-G-Si	15	0.075
	20	0.10
	25	0.125
PA-*T*-Si	20	0.1

[#] Over total mass of supracolloidal coatings.

nanoparticles covalently bound to the polymer particles, PEO chains grafted on the polymer cores, low surface grafting density of thiol groups on silica nanoparticles, and a 20 wt% fraction of silica nanoparticles initially added to the aqueous dispersion. The description of the particles used to prepare the coatings is shown in Table 2. The coatings were prepared as free-standing films by casting the dispersions on Teflon sheets and drying under air flow and room temperature for a determined period, see Methods for details.

3.1.2. *Physical adsorption versus chemical binding on the supracolloids*

The core-corona morphology of polymer-silica supracolloids strongly depends on the pH of the dispersion. Silica nanoparticles can detach from the polymers and/or freely exchange between polymer surfaces with changes in the medium, namely at pH higher than 10. [43,44,49] This dynamic adsorption of the silica particles and possible disturbance of the corona configuration may become an issue during the formation of water-borne coatings, for example, the drying process is often accompanied by a pH change. Hence to circumvent possible instabilities and loss of the core-corona morphology during film preparation, we prepared two types of polymer-silica supracolloids: One in which the silica nanoparticles are solely physically adsorbed on the polymer surface (PA-G-Si series), and one where the silica nanoparticles are covalently bound to the polymer surfaces (CB-G-Si) via disulfide bonds, to covalently fix the strawberry morphology.

To confirm the type of bond/interaction between the particles in the assemblies, the supracolloidal dispersions were subjected to a pH variation using a sodium hydroxide solution. The PA-G-Si.20 dispersion initially assembled at pH 9.5 showed a hydrodynamic diameter of ≈ 550 nm which corresponds well with the formation of a strawberry assembly, Fig. 1a. However, when the pH was raised to 11.5 a significant decrease in the hydrodynamic diameter was observed down to ≈ 269 nm, which is close to the hydrodynamic diameter of the core polymer particles alone (G.24, see Table 1). This indicates that full dissociation of the silica nanoparticles from the surfaces of polymer particles took place. The comparison of cryo-TEM images of the dispersions at pH 9.5 and 11.5 further confirm this disassembly with pH increase, Fig. 1b.

For the CB-G-Si.20 supraparticles, similar strawberry assemblies were obtained at pH 9.5. Although the initial hydrodynamic diameter of CB-G-Si.20 was slightly larger than for PA-G-Si.20, there is no evidence from the cryo-TEM images of agglomerates in the dispersion (Fig. 1b). It should also be noted that the zeta potential at pH 9.5 is around −50 mV for both dispersions, which is an indication of initially stable supracolloidal dispersions[50]. When the pH was increased to 11.5 for CB-G-Si.20, only a slight variation of the hydrodynamic diameter was detected and the zeta potential remained rather constant. On the opposite, for PA-G-Si.20, the hydrodynamic diameter dropped nearly two-fold and the zeta potential increased to −15 mV (Fig. 1a). These results indicate that the CB-G-Si.20 supracolloids do not disassemble and remain stable with increasing pH. This is further confirmed by the strawberry assemblies shown in the cryo-TEM images at pH = 11.5 (Fig. 1b), where only some minor free silica nanoparticles can be observed in the medium. As expected, the covalent disulfide bonds formed between the polymer-silica surfaces on the CB-G-Si.20 dispersions (Scheme 1B) are not sensitive to the pH increase, contrary to the silica-polymer (PEO) pH-sensitive adsorption interactions that hold the assemblies together in the PA-G-Si.20.

3.1.3. *Silica distribution and nanostructures on/in the coatings*

Transparent and colorless coatings were obtained from all supracolloidal dispersions. The coatings prepared from CB-G-Si.20 had a smooth appearance as compared to the heavily wrinkled PA-G-Si.20 films, see Fig. S1. This dissimilar surface appearance hinted at a different nanostructure and/or chemical composition of the air-coating interface. ATR-FTIR was used to investigate the surface chemical composition of these two coatings. Fig. 2 shows the spectra of the air-coating and substrate-coating interfaces for both coatings. For CB-G-Si.20 the spectra of the two interfaces largely overlapped indicating a similar chemical composition at the air and substrate interfaces, Fig. 2a.

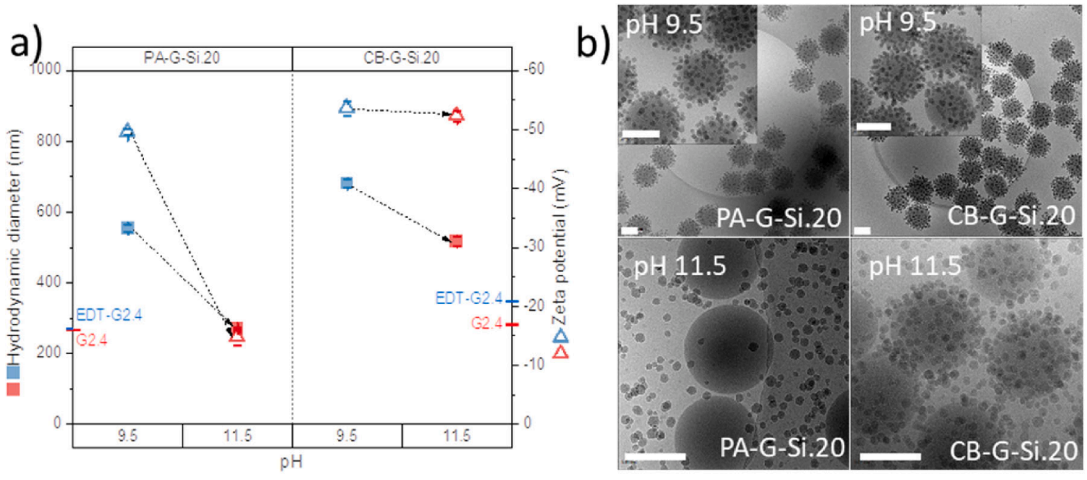

Fig. 1. Ph influence on physically adsorbed and covalently fixed strawberry supracolloids - a) Average hydrodynamic diameter and zeta potential *versus* pH of PA-G-Si.20 and CB-G-Si.20 supracolloidal dispersions. The ticks on the *y* axes indicate the hydrodynamic diameter (left) and zeta potential (right) of EDT-G2.4 polymer dispersion at pH 9.5 (blue) and of the G2.4 polymer dispersion at pH 11.5 (red). b) Cryo-TEM images of the respective dispersions prepared at pH 9.5 and pH 11.5. (Scale bars = 200 nm). (For interpretation of the references to color in this figure legend, the reader is referred to the web version of this article.)

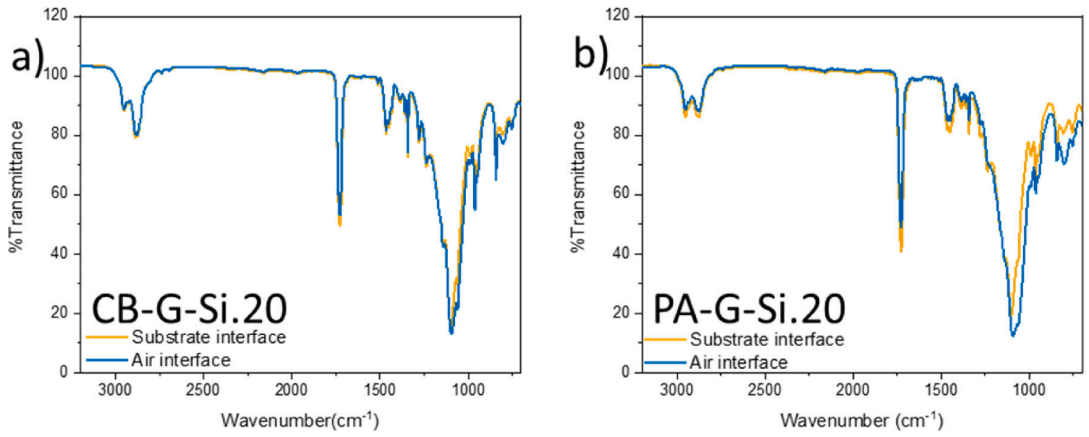

Fig. 2. Chemical composition of the supracolloidal films - ATR-FTIR spectra of (a) CB-G-Si.20 and (b) PA-G-Si.20 free-standing coatings, air, and substrate interface.

For PA-G-Si.20, however, several differences can be identified between the two interfaces, see Fig. 2b. When compared to the substrate-coating interface, the air-coating interface showed a significantly stronger absorbance at 1100 cm^{-1}, corresponding to the $\upsilon_{Si\text{-}O}$ vibration band (SiO_2 nanoparticles), and a lower absorbance at 1700 cm^{-1}, corresponding to the $\upsilon_{C=O}$ vibration band of the acrylate groups of the polymer core. This indicates the air interface of the PA-G-Si.20 coating is highly enriched with silica nanoparticles and depleted from polymer particles. Furthermore, it can also be seen in Fig. 2 that for CB-G-Si.20 coatings the $\upsilon_{(O\text{-})C\text{-}H}$ vibration band at 2880 cm^{-1}, associated with the carboxyl and ether groups of the polymer particles, was significantly more intense than the band at 2950 cm^{-1}, attributed to $\upsilon_{(C\text{-})C\text{-}H}$, when compared to PA-G-Si.20. This may indicate that there is probably more PEO at interfaces of the CB-G-Si.20 coating. A possible explanation is that the crosslinking between silica and the poly(BA-*co*-MMA) core surface reduces the adsorption of free PEO chains (from Triton). Accordingly, the PA-*T*-Si.20 coating was observed to have a higher absorbance at 2880 cm^{-1} (Fig. S2b). The effect of free surfactant on the coatings properties is further discussed in the water sensitivity section. Although these ATR-FTIR measurements indicate that there is surface segregation of silica nanoparticles in the PA-G-Si.20 films, these measurements only provide information on the top ≈ 1 μm[51] close to the air interface, which is much less than the overall thickness of supracolloidal coatings (≈ 80–100 μm). To investigate the distribution of particles and structures throughout the bulk of the coatings, the free-standing films were frozen and manually cracked. Their cross-section was analyzed with Scanning Electron Microscopy (SEM), Fig. 3. The cross-sections of coatings with other silica weight fractions (Si.xx) are

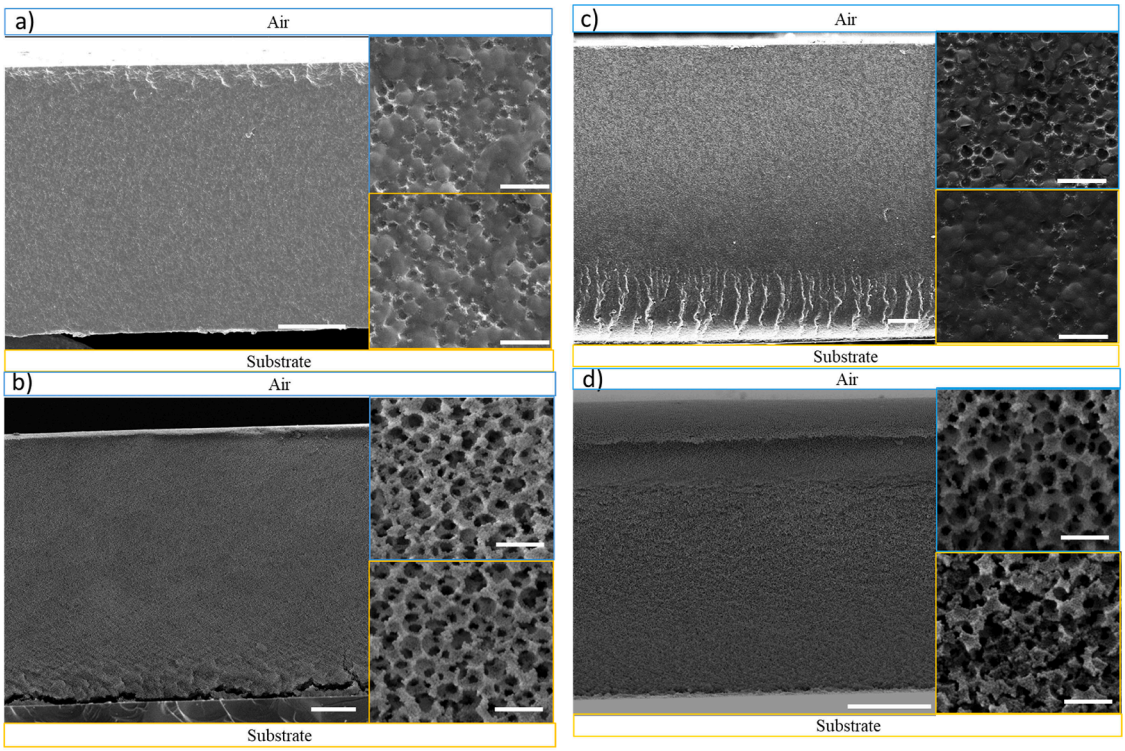

Fig. 3. Depth profile imaging of the supracolloidal coatings – SEM images of the cross-sections of the supracolloidal films before, and after calcination: CB-G-Si.20 (a, b, respectively) and PA-G-Si.20 (c, d, respectively). The images are representative cross-sectional areas of the overall film length/thickness (Scale bars = 10 μm). *Insets*: High magnification images of the cross-section near the air-coating (*top, blue frame*) and substrate-coating interfaces (*bottom, yellow frame*), (Scale bars = 1 μm). (For interpretation of the references to color in this figure legend, the reader is referred to the web version of this article.)

shown in Fig. S3.

The depth profile of the CB-G-Si.20 film does not show any significant contrast difference along the cross-section of the film (Fig. 3a). The higher magnification images of the air- and substrate-coating interfaces (*insets* of Fig. 3a) clearly show the presence of the supracolloidal structures, with the silica nanoparticles at the boundaries of the polymer particles. Silica and polymer particles seem to form a continuous (nano) network that is homogeneously reproduced throughout the film and at the interfaces. To further analyze the distribution of the silica nanoparticles, the coatings were calcinated under air at 600 ℃. SEM images of the calcinated films showed a continuous silica nanoparticles skeleton structure which further confirmed the uniform distribution of the silica nanoparticles on a continuous 3D network throughout the CB-G-Si.20 coating (Fig. 3b). This seems to be related to the fact that the nanoparticles are covalently bound into the assemblies and remain so during the drying of the films, even when pH increases. As the film dries the strawberry assemblies pack in a semi-ordered way which is highly relevant to the special optical properties of supracolloidal coatings, and the coating ends up with a uniform distribution of the silica nanoparticles throughout its height, and at the interfaces.

For the PA-G-Si.20 coatings there is, however, a large contrast along the film cross-section. Near the air interface, the film showed a brighter region which spans over more than 30 μm toward the inside of the coating (Fig. 3c). This result suggest that there is a higher density of silica nanoparticles near the air interface which is a clear indication of stratification of the silica nanoparticles at this interface. Typically, heavier chemical elements like silicon with larger nuclei can deflect incident electrons more strongly than lighter elements, like carbon and hydrogen, giving higher contrast. This leads to brighter regions in SEM images. Higher magnification images of the cross-section of air and substrate interfaces (*insets* of Fig. 3c) also show the regional disparity of silica nanoparticles concentration (bright region) between the interfaces. This is further confirmed by the non-uniform and irregular silica nanoparticles skeleton formed throughout the cross-section, after removing the polymer cores by calcination (Fig. 3d). The bright region near the substrate interface (Fig. 3c) is somehow underlined by the artifacts or "dendritic structures" present in that area, which are artifacts created during the freeze-break procedure applied to the samples when preparing the cross-sections for SEM (described in section 2.6). Besides, it is possible that a very thin, a few microns only, silica-rich phase formed at the substrate interface by sedimentation of free silica nanoparticles during the long drying process. Besides, the thickness of PA-G-Si.20 film is strongly diminished after the calcination while CB-G-Si.20 had only a few micrometers variation. The formation of the percolating silica network via the covalently bound supracolloids prevents the collapse of the cross-section upon burning of the polymer phase and reduction of the thickness (Fig. S4).

Even though both CB-G-Si.20 and PA-G-Si.20 initial dispersions consisted of similar strawberry supracolloids, their coatings ended up with a very different distribution of the silica nanoparticles and bulk structures. In the previous section, it was shown that the increase in pH strongly affects the stability of the PA-G-Si.20 dispersions. One hypothesis for the stratification of the silica nanoparticles on these coatings can be explained as follows. During the drying process, water evaporates and the pH and ionic strength of the applied film increase. This results in the disassembly of the supracolloids and the release of a large number of free silica nanoparticles into the medium of the wet/drying coating. The Peclet number (*Pe)* for both particles in this system are larger than 1 ($Pe_{polymer} > Pe_{Si} > 1$), (calculations provided in SI, Table S1). In this situation, the diffusion of the particles is too slow in relation to the water evaporation, which causes the particles to become entrapped at the drying/receding interface.[52,53] Furthermore, since the *Pe* of the polymer particles is much larger than the one of the silica nanoparticles there is a concentration gradient of particles along the height of the wet film, which generates an osmotic pressure gradient and forces some of the particles away from the liquid/air interface. This diffusiophoresis phenomenon, observed by Luo *et al.*[54] and later studied by Fortini *et al.*[33], has a greater effect on larger particles which results in a small-on-top film inner structure. Hence, the silica nanoparticles are preferentially directed/accumulated at the air interface in relation to the polymer particles, which is exactly what we observe from the characterization of the PA-G-Si.20 coatings (Fig. 2b, Fig. 3c and d). Further studies on this segregation mechanism occurring in bi-modal dispersions were reported by Sear and Warren[55] and Martín-Fabiani *et al.*[36].

Another hypothesis could explain/contribute to the silica stratification observed in the PA-G-Si.20 coatings only, relates to the presence of free PEO chains from the stabilizer Triton X-405 used in the emulsion polymerization (Table 2). For relatively low pH, there is a strong attraction between PEO chains and silica particles in an aqueous solution.[56,57] During the drying of the film and water evaporation, the free PEO chains in the dispersion may instantaneously adsorb at the interfaces of the applied/wet film. Due to the interaction of silica/PEO being stronger than silica/water this interfacial layer of adsorbed surfactant could provide a more favorable environment for any free silica nanoparticles (released by disassembly) to accumulate at the interfaces.[58] Further on, the silica/PEO adsorption attraction is also larger than the polymer/PEO hydrophobic attraction which could further drive the silica disassembly from the strawberry assemblies in the PA-G-Si.20 coatings, pushing the polymer particles together. It should be noted that a strong stratification of the silica nanoparticles was also observed on coatings prepared from supracolloidal dispersions assembled via physical adsorption, with free PEO chains from Triton only (PA-*T*-Si.20), *i.e.*, no PEO-polymer grafted chains, shown in Figure S2 and S6.

The distribution of silica nanoparticles throughout the coatings layer was further characterized by analyzing the cross-section of the film with EDX and ATR-FTIR in reflection mode with a "pseudo" in-depth resolution. Fig. 4a shows that the relative silicon atomic concentration fluctuated only slightly over the depth profile of the CB-G-Si.20 coating, which confirms the uniform distribution of the silica nanoparticles from the air to the substrate interface. In contrast, for the PA-G-Si.20, the silica nanoparticles concentration near the air-coating interface is much higher than for CB-G-Si.20, it then drastically decreases towards the middle of the coating, and finally approaches a plateau region near the substrate interface, at a lower value than for CB-G-Si.20. These results confirm in a semi-quantitative way the conclusions derived above from the SEM images and indicate that we have an effective method to quantify the silica distribution along the depth profile in the supracolloidal films. As expected, for the PA-*T*-Si.20 coatings, obtained from supracolloidal dispersions assembled with only free PEO chains, the silicon profile also denotes stratification, Fig. 4a. When compared to the PA-G-Si.20 coatings, a rather linear decrease in silica concentration was observed and the initial silica concentration near the air-coating interface is higher (Fig. 4b and S6). The slightly higher silica content near the air- and substrate-coating interface of CB-G-Si.20 might be attributed to the stratification and sedimentation of free silica nanoparticles, respectively. In conclusion, clear evidence and a supported hypothesis have been put forward here for the silica stratification on the physically adsorbed supracolloidal films, however, the exact stratification mechanism requires further exploration, for example by adjusting the drying parameters such as humidity and temperature or the strength of physical interactions (Figure S6) and will be addressed elsewhere.

3.2. Properties of supracolloidal coatings

3.2.1. Mechanical properties

Since CB-G-Si and PA-G-Si supracolloidal coatings exhibited very different silica distributions throughout the bulk, we evaluated the influence of these nanostructures on their thermo-mechanical properties.[59] The storage modulus G', loss modulus G'' and loss factor tan δ were obtained by temperature sweeps measured using a plate-plate rheometer. This setup allows overcoming the limitation of measuring a soft polymer film at a temperature higher than 50 ℃ and the inhomogeneous

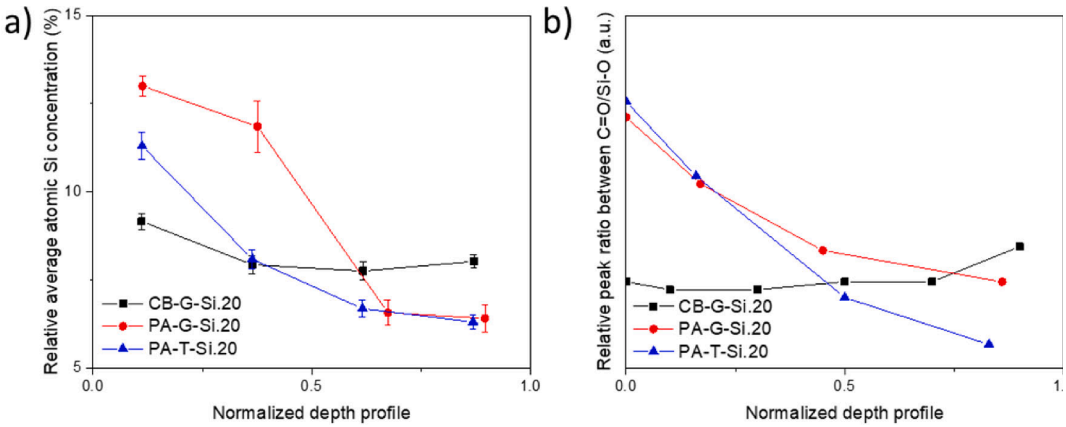

Fig. 4. Depth-resolved chemical analyses of the supracolloidal coatings - a) Relative silicon atomic concentration over the depth profile (a.u.) calculated from EDX and **b)** Relative ratio of the $\upsilon_{SiO/CO}$ height over the depth profile estimated from ATR-FTIR. *Zero* and *one* are the air- and substrate-coating interfaces, respectively.

silica depth profile present in some of the coatings.

All the supracolloidal films, both physically adsorbed and covalently bound, show a very significant increase of the storage modulus G' compared to coatings obtained from polymer particles only (G2.4 and EDT-G2.4) (Fig. 5a and b), revealing that the incorporation of the silica nanoparticles effectively improved the elastic properties of the films within the rubbery region. These observations were also reported for other similar systems [40,60]. The relative storage modulus G'_r of nanocomposite coatings and materials with well-dispersed nanofillers can be predicted by the Einstein-Smallwood (ES) equation,

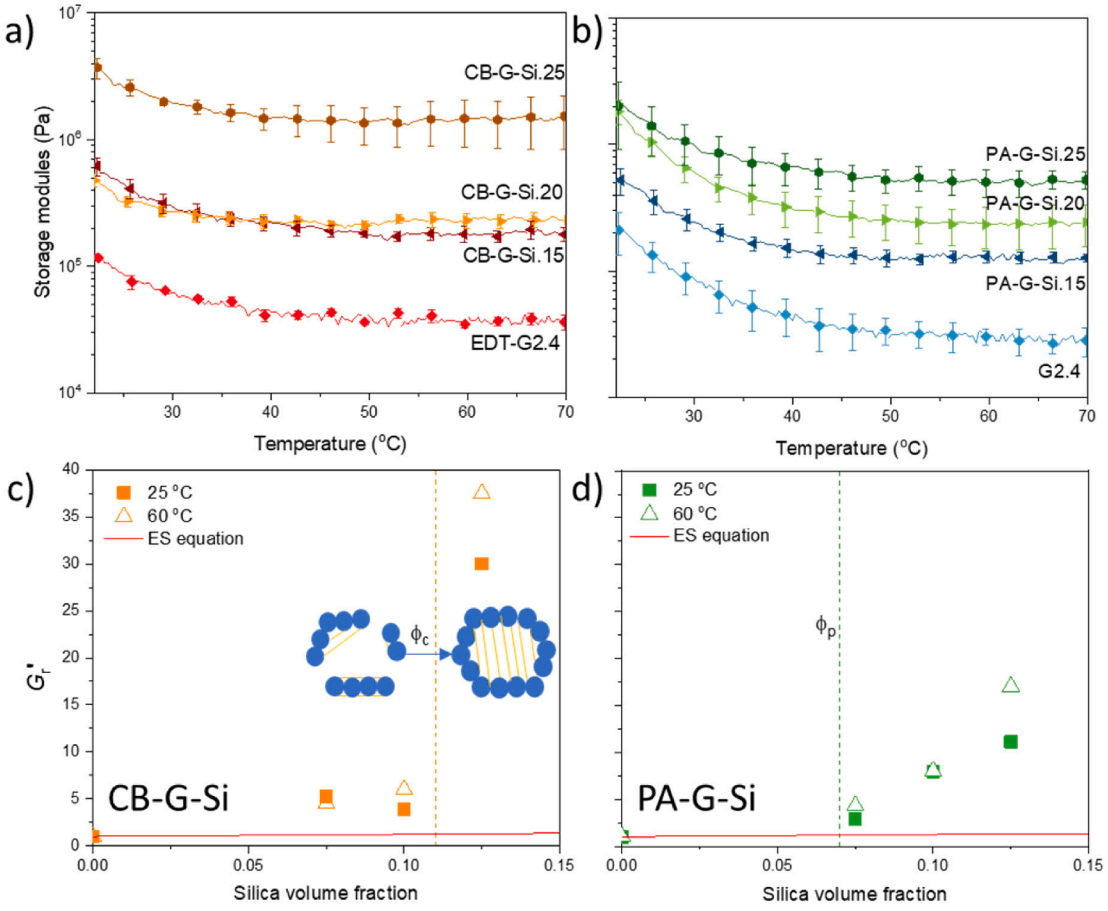

Fig. 5. Analyses of the storage moduli of the supracolloidal coatings - Storage moduli (G') of (a) chemically bound and (b) physically adsorbed supracolloidal films. Measured relative storage moduli G'_r *versus* silica volume fraction ϕ_{Si} at 25 ℃ and 60 ℃, for (c) chemically bound and (d) physically adsorbed supracolloidal films. The horizontal solid-red line represents the G'_r of equivalent nanocomposites as predicted by Einstein-Smallwood (ES) equation. The vertical dash-orange line indicates the approximate critical volume fraction (ϕ_c) of the supracolloidal coatings. The vertical dash-green line indicates the theoretical percolating volume fraction (ϕ_p). The inset scheme shows the volume transition of shear-shielded polymer (*yellow strips*) with silica (*blue circles*) volume fraction increased from $\phi_{Si} \geqslant \phi_p$ to $\phi_{Si} \geqslant \phi_c$. (For interpretation of the references to color in this figure legend, the reader is referred to the web version of this article.)

$$G_r^{'} = \frac{G_{\text{filled}}^{'}}{G_{\text{polymer}}^{'}} = 1 + 2.5\phi_{\text{filler}} \quad (5)$$

where $G_{\text{filled}}^{'}$ is the storage modulus of the nanofilled polymer coating, $G_{\text{polymer}}^{'}$ is the storage modulus of the polymer (only) coating and ϕ_{filler} is the volume fraction of nanofillers.[61] This relation has been demonstrated to be only valid for nanocomposites below the percolation concentration, above which the particles form a space-spanning network. A percolating inorganic network and the adsorbed/immobilized polymer layer at the surface of fillers can strongly contribute to the mechanical reinforcement of the coatings.[62–64] In Fig. 5c and d we plotted the relative storage moduli $G_r^{'}$ (based on the measured $G^{'}$ values) *versus* the silica volume fraction of the supracolloidal coatings at 25 °C and 60 °C. For all CB-G-Si coatings the measured $G_r^{'}$ were higher than the $G_r^{'}$-ES prediction (Fig. 5c, solid red line). This strongly indicates the presence of a percolated silica network which contributes to an enhancement of storage modulus, *i.e.*, a coatings reinforcement. The theoretical percolating volume fraction ϕ_p of the supracolloidal coatings was estimated as 0.07 (calculation in SI based on the approach developed by Kusy[65]). Since all coatings were made with a silica volume fraction higher than this value, they are indeed expected to grow several folds on storage moduli compared to the ES equation predicted value, due to the contribution of the hydrodynamic effect of a percolated network.

Fig. 5c further shows, however, that only for CB-G-Si.25 (ϕ_{Si} = 0.125), the domain continuous phase shifted from polymer to silica, which exceedingly contributes to the reinforcement of the coatings.[66,67] This could be attributed to higher silica-silica contact points and/or a smaller network mesh size (schematic in Fig. 5c). According to relevant literature, it seems reasonable to assume that above a critical silica volume fraction (ϕ_c) the enhancement of $G^{'}$ was further independent of the silica mass fraction.[66–68] In these coatings the ϕ_c is expected to be between 0.1 and 0.125 (represented by orange vertical dash lines in Fig. 5c). It is also worth noticing that ϕ_c of these coatings are much lower in comparison to silica-rubber systems with well-dispersed nanoparticles, or simple binary colloidal mixtures reported in the literature. This clearly illustrates the superior properties of the CB-G-Si supracolloidal coatings, mainly due to its close packing of supracolloids which results in 3D networks of silica nanoparticles with a small mesh size.[62,66].

For PA-G-Si coatings, the measured $G_r^{'}$ showed a clearly different behavior with an almost linear relation with increasing ϕ_{Si} (Fig. 5d). Due to the heterogeneous distribution of silica nanoparticles in these supracolloidal coatings, the densely stratified silica networks domain near the interfaces could contribute to the mechanical reinforcement. Hence, the $G_r^{'}$ was a result of the averaged contribution of a silica network with different mesh sizes, from the air toward the substrate interface of the coatings. With the increase of silica mass fraction, probably the total (average) volume of the silica network that met the ϕ_c increased, which lead to a near-linear relation between storage moduli and ϕ_{Si} fraction. The loss moduli and loss factor of supracolloidal coatings were available and discussed in SI (Figure S9 and S10).

3.2.2. *Water resistance of supracolloidal films*

The results reported in the previous section (Fig. 2) suggest that the crosslinking of the particles might exclude the PEO chains from the silica surfaces, favoring their segregation towards the coatings interfaces or potentially inside the coatings, forming inner clusters. These effects caused by crosslinking can eventually change the water sensitivity of the films. Note that a low water vapor uptake (WVU) is required for high-performance water-borne coatings.

The WVU of the supracolloidal films was analyzed with dynamic vapor sorption (DVS). The original (non-normalized) mass change (%) at different relative humidity (RH) ranges is provided in Fig. S10 for all coatings. All CB-G-Si, PA-G-Si, and G2.4 showed similar WVU throughout the measured humidity range with values comparable to other water-barrier coatings.[69] All measured films showed a type III isotherm in the Brunauer-Emett-Teller (BET) adsorption model, where the reactive sites allow for the adsorption of an infinite amount of water molecules, indicating that there could be water condensation either within mesopores or on the surface.[70].

It can be assumed that the embedded non-porous silica nanoparticles can hardly take up any water vapor by absorption. Hence, the WVU of the supracolloidal films was normalized to the polymer mass fraction in supracolloidal coatings and measured at 95% RH (Fig. 6a) to study the effect of the silica incorporation on the WVU of the nanocomposite films. The CB-G-Si films exhibit a higher WVU than the respective polymer film alone (G2.4). This observation further supports the hypothesis of an increased film porosity in the supracolloidal films. It should be noted that the EDT-G2.4, crosslinked film obtained from polymer particles alone, showed a slightly lower WVU than the G2.4 film. Hence, the increase of WVU in the supracolloidal films can be indeed attributed to the chemical binding between polymer and silica nanoparticles. Furthermore, the WVU increase correlates positively with the increasing silica concentration in the CB-G-Si series (Fig. 6a).

For the PA-G-Si films, the WVU was close to values measured for the polymer film alone (G2.4) within the error margin, revealing that neither the silica stratification nor the eventual presence of free/mobile silica nanoparticles had a significant influence on the film's porosity. A coating made from polymer particles only and stabilized by free PEO chains (T4.6) showed a higher WVU as compared to G2.4. Since both polymer films have a similar mass fraction of PEO segments, this suggests that the free PEO chains (from Triton surfactant) had a higher contribution to the WVU compared to the grafted PEO (from PEGMA). The free PEO chains might aggregate in CB-G-Si supracolloidal coatings and adsorb a higher amount of water vapor compared to the PEO presented at particles surface. Furthermore, the higher water vapor uptake measured for a PA-*T*-Si.20 film as compared to T4.6 (Fig. 6a) can be explained by the stratification of silica nanoparticles towards the interfaces, which might result in a layer of PEO chains at the air-film interface and create more surface-active sites for the water condensation at the film surface.

The water diffusion coefficient (D_{water}) of the films was also investigated, by monitoring the constant mass change rate (dm/dt) region before the equilibrium is reached at each humidity value measured (Fig. 6b).[71] For the polymer films G2.4, EDT-G2.4, and T.46, D_{water} started to decrease above 30% RH. However, for the supracolloidal films, it only dropped from 85% RH onwards. This decrease can be explained as the partial self-diffusion of water due to the water saturation into the pores of the films. Small pores become saturated at lower humidity values as compared to larger pores. This is in good agreement with the WVU of the supracolloidal films and the hypothesis postulated above. The supracolloidal films should have a higher porosity compared to the polymer films only, due to silica nanoparticles disturbing the interdiffusion of the polymer chains.

EDT-G2.4 and T.46 polymer films showed a similar D_{water}, while G.24 showed the highest value of all films. This result suggests that the presence of grafted-PEGMA brushes at the polymer particles interface benefits the transport of water molecules throughout the films when compared with polymer particles made with free PEO chains (Triton) only.

All PA-G-Si and CB-G-Si films showed similar D_{water} below 80% humidity, which indicates that the water transport through the films, as well as their porosity, is rather similar. Thus, it is reasonable to state that the high WVU observed for the CB-G-Si films is mainly due to the exclusion of free PEO chains towards the film interfaces, which provided more reactive sites for water to adsorb and condense on the film air interface (visually confirmed, see Fig. S13). The water permeability of all films measured by the dry-cup method is provided in SI (Fig. S11d) and shows that the diffusion of water through the supracolloids coating can be described using Fick's diffusion law.

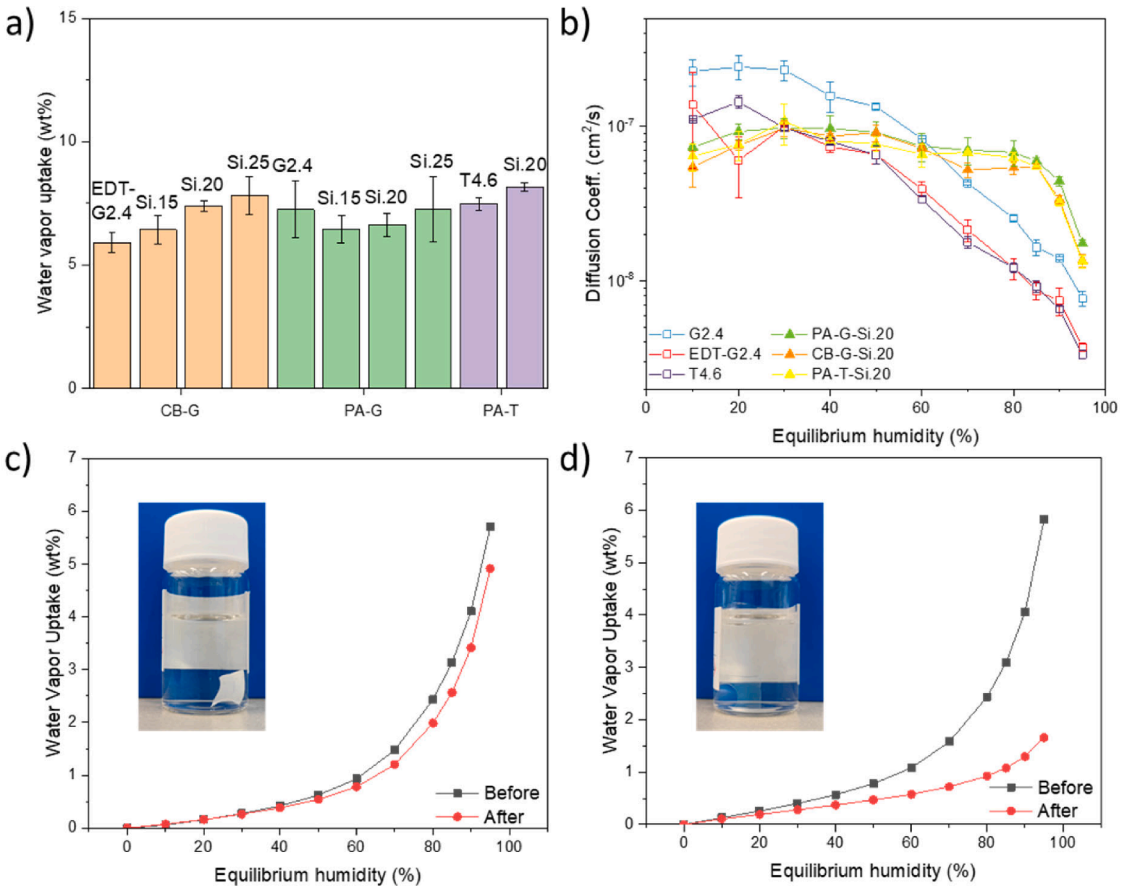

Fig. 6. Water uptake of and water diffusion coefficient in supracolloidal films, before and after washing with deionized water - (a) Water vapor uptake of original coatings at 95% humidity normalized to the polymer mass fraction in the supracolloidal coatings. (b) Diffusion coefficient of original coating at different humidity values. Water vapor uptake profile of c) EDT-G2.4 and d) CB-G-Si.20 coatings before and after washing with deionized water. *Insets* - Digital photographs of films after being soaked in water for 2 days.

To provide additional support for the discussion above, selected films were washed in deionized water for 2 days (see experimental), dried up, and measured again in DVS (Fig. 6c and d). The WVU of the washed polymer films (EDT-G2.4), only shows slight fluctuations when compared with the unwashed films, which indicates that the porosity of the films is similar and remains the same after long time immersion in water. The washed supracolloidal films, CB-G-Si.20, PA-G-Si.20 and PA-*T*-Si.20 films, showed a similar WVU over the whole humidity range which is, however, remarkably reduced as compared to the unwashed films (example in Fig. 6d, others in Fig. S14). Furthermore, the adsorption isotherm changed from type III to type II, indicating that there are more active water absorption sites on the unwashed films. This is confirmed by the D_{water} measured for the washed films which slightly increases compared to non-washed films, indicating that the free PEO may have been washed away and/or the porosity of the film slightly increased (Fig. S14c).

As a last remark, the CB-G-Si.20 film immersed in water (*inset* Fig. 6d) showed angle-dependent light green reflection, which is an indication that water interacted in the pores at well-arranged ordered silica-polymer interfaces, which changed the reflection index of the supracolloids interfaces. These films with changing color upon water immersion may have further potential applications which will be explored in other works, such as in flexible humidity sensors (video showing the reflecting colors provided in SI).[72].

4. Conclusions

Polymer-silica supracolloidal nanocomposites have been recurrently used to control the distribution of inorganic nanofillers on water-borne coatings and improve the coatings performance[3,5,18–23,42,43] However, a good compromise between reasonable film formation properties (*i.e.*, sufficient mobility for polymer chains interdiffusion), low aggregation of the nanofillers, and the build-up of percolating fillers networks which improve the coatings performance, remains difficult to achieve.

In this work we devised a strategy to obtain this compromise for water-borne polymer coatings containing silica nanoparticles as fillers, by using supracolloidal particles which have covalently bonded units and simultaneously promote additional crosslinking of the coatings. We used concentrated aqueous dispersions of polymer-silica supracolloids with strawberry configuration to prepare water-borne coatings with different distribution of the inorganic fillers. To ensure that the strawberry assemblies remain in this configuration during drying of the aqueous dispersions, we introduced covalent-disulphide bonds between the colloidal units. These chemical moieties were also used to further crosslink the coatings via oxidation in air. For comparison we also prepared coatings from our previous physically adsorbed strawberry supracolloids [44]. A significantly different distribution of the silica nanoparticles was observed in the coatings prepared from supracolloids simply stabilized by physical adsorption [44] or held together by covalent bonds. For the first, a heavy stratification of the silica nanoparticles towards the air and substrate interfaces was observed while for the second well-arranged homogenous and percolating 3D silica nanonetworks were present throughout the coating.

The storage modulus of the supracolloidal coatings containing these nanonetworks was up to 30 times higher than the values of comparable

films made from polymer only, and of similar films reported in literature with fillers of comparable size. [64] The extraordinary mechanical reinforcement effects, namely on the covalently bound supracolloidal films were explained based on the predominance of silica network as the continuous phase and the hydrodynamic effect provided by the percolating silica network. The incorporation of the silica nanonetwork also enhanced the water resistance of the coatings, hence they remain transparent even in high humidity conditions or contact with water (no opaqueness development). Furthermore, when these silica-polymer coatings interact directly with water, upon immersion, they show angle-depended structural color (green). Hence, the supracolloidal films with highly controlled 3D networks of the silica nanoparticles provide high potential for practical applications where water-borne coatings with strong mechanical properties may be required, such as in optical, sensory, selective separation, and catalytical applications.

Declaration of Competing Interest

The authors declare the following financial interests/personal relationships which may be considered as potential competing interests: Siyu Li reports financial support was provided by Advanced Research Center Chemical Building Block Consortium (ARC CBBC) to cover her PhD work, in the form of a research grant. The grant was processed via our institution, Eindhoven University of technology. All rights on the current work belong to the authors and the University.

Data availability

Data will be made available on request.

Acknowledgements

The authors are grateful for the financial support from the Advanced Research Center for Chemical Building Blocks, ARC CBBC, which is co-founded and co-financed by the Dutch Research Council (NWO) and the Netherlands Ministry of Economic Affairs and Climate Policy. Dr. Gerard van Ewijk (AkzoNobel), Dr. Daniel Persson (Nouryon), Dr. Keimpe van der Berg (AkzoNobel), Dr. Per Restorp (Nouryon), Dr. Heiner Friedrich and Dr. Bart J.F. Erich are acknowledged for their useful insights and discussions. Akal D. Aras and Rick R.M Joosten are thanked for their assistance with water permeability and cryo-TEM measurement, respectively. Pauline Schmit is acknowledged for her assistance with cryo-microtoming of the coating sections for depth-resolved IR.

Authors Contribution

S. Li prepared the supracolloids dispersion and coatings, performed cryo-TEM, SEM, DLS, ATR-FTIR, DMTA, and DVS experiments, and analysed the data. A.B. Spoelstra performed the ultra-low-angle-cryo-microtoming of supracolloidal films. A. C. C. Esteves conceived the research idea and did the main supervision of the research work. R. Tuinier and L. G. J. van der Ven contributed to the work supervision. All authors contributed to the data interpretation via discussions, and to the (partial) writing and/or revision of the manuscript.

Appendix A. Supplementary data

Supplementary data to this article can be found online at https://doi.org/10.1016/j.jcis.2023.04.154.

References

[1] J.A. Graystone, Coatings for Buildings, Paint and Surface Coatings (1999) 330–410.
[2] H. Althues, J. Henle, S. Kaskel, Functional Inorganic Nanofillers for Transparent Polymers, Chem. Soc. Rev. 36 (9) (2007) 1454–1465.
[3] B.M. Novak, Hybrid Nanocomposite Materials?Between Inorganic Glasses and Organic Polymers, Adv. Mater. 5 (6) (1993) 422–433.
[4] T. Wang, J.L. Keddie, Design and Fabrication of Colloidal Polymer Nanocomposites. Advances in Colloid and Interface Science, Elsevier 1 (March 2009) 319–332.
[5] H. Zou, S. Wu, J. Shen, Polymer/Silica Nanocomposites: Preparation, Characterization, Properties, and Applications, Chem. Rev. 108 (9) (2008) 3893–3957.
[6] E. Chabert, M. Bornert, E. Bourgeat-Lami, J.Y. Cavaillé, R. Dendievel, C. Gauthier, J.L. Putaux, A. Zaoui, Filler-Filler Interactions and Viscoelastic Behavior of Polymer Nanocomposites, Mater. Sci. Eng. A 381 (1–2) (2004) 320–330.
[7] D.W. Schaefer, R.S. Justice, How Nano Are Nanocomposites? Macromolecules 40 (24) (2007) 8501–8517.
[8] M. Tatou, A.-C. Genix, A. Imaz, J. Forcada, A. Banc, R. Schweins, I. Grillo, J. Oberdisse, Reinforcement and Polymer Mobility in Silica-Latex Nanocomposites with Controlled Aggregation, Macromolecules 44 (22) (2011) 9029–9039.
[9] Y. Li, X. Huang, L. Zeng, R. Li, H. Tian, X. Fu, Y. Wang, W.H. Zhong, A Review of the Electrical and Mechanical Properties of Carbon Nanofiller-Reinforced Polymer Composites, J. Mater. Sci. 54 (2) (2019) 1036–1076.
[10] P.C. Ma, N.A. Siddiqui, G. Marom, J.K. Kim, Dispersion and Functionalization of Carbon Nanotubes for Polymer-Based Nanocomposites: A Review, Compos. A Appl. Sci. Manuf. 41 (10) (2010) 1345–1367.
[11] C. Sanchez, K.J. Shea, S. Kitagawa, F.M. Kerton, M. Pagliaro, M. Rossi, T. Perchyonok, Applications of Advanced Hybrid Organic-Inorganic Nanomaterials: From Laboratory to Market, Chem. Soc. Rev. 40 (2) (2011) 696–753.
[12] P.T. Elliott, J.E. Glass, Water-Born Coatings, in: Applied Polymer Science: 21st Century, Elsevier, 2000, pp. 563–588.
[13] J.L. Keddie, A.F. Routh, Fundamentals of Latex Film Formation; Springer Laboratory; Springer Netherlands: Dordrecht, 2010.
[14] F. Lecomte, J. Siepmann, M. Walther, R.J. MacRae, R. Bodmeier, Polymer Blends Used for the Coating of Multiparticulates: Comparison of Aqueous and Organic Coating Techniques, Pharm. Res. 21 (5) (2004) 882–890.
[15] J.C. Grunlan, A.R. Mehrabi, M.V. Bannon, J.L. Bahr, Water-Based Single-Walled-Nanotube-Filled Polymer Composite with an Exceptionally Low Percolation Threshold, Adv. Mater. 16 (2) (2004) 150–153.
[16] Z. Qian, Z. Zhang, L. Song, H. Liu, A Novel Approach to Raspberry-like Particles for Superhydrophobic Materials, J. Mater. Chem. 19 (9) (2009) 1297–1304.
[17] J.A. Balmer, A. Schmid, S.P. Armes, Colloidal Nanocomposite Particles: Quo Vadis? J. Mater. Chem. 18 (47) (2008) 5722–5730.
[18] M.J. Percy, S.P. Armes, Surfactant-Free Synthesis of Colloidal Poly(Methyl Methacrylate)/Silica Nanocomposites in the Absence of Auxiliary Comonomers, Langmuir 18 (12) (2002) 4562–4565.
[19] F. Tiarks, K. Landfester, M. Antonietti, Silica Nanoparticles as Surfactants and Fillers for Latexes Made by Miniemulsion Polymerization, Langmuir 17 (19) (2001) 5775–5780.
[20] E. Bourgeat-Lami, J. Lang, Encapsulation of Inorganic Particles by Dispersion Polymerization in Polar Media, J. Colloid Interface Sci. 197 (2) (1998) 293–308.
[21] A. Schoth, K. Landfester, R. Muñoz-Espí, Surfactant-Free Polyurethane Nanocapsules via Inverse Pickering Miniemulsion, Langmuir 31 (13) (2015) 3784–3788.
[22] A. Schmid, J. Tonnar, S.P. Armes, A New Highly Efficient Route to Polymer-Silica Colloidal Nanocomposite Particles, Adv. Mater. 20 (17) (2008) 3331–3336.
[23] K. González-Matheus, G.P. Leal, J.M. Asua, Film Formation from Pickering Stabilized Waterborne Polymer Dispersions, Polymer 69 (1) (2015) 73–82.
[24] N. Negrete-Herrera, J.L. Putaux, L. David, F. de Haas, E. Bourgeat-Lami, Polymer/Laponite Composite Latexes: Particle Morphology, Film Microstructure, and Properties, Macromol. Rapid Commun. 28 (15) (2007) 1567–1573.
[25] A. Schoth, C. Wagner, L.L. Hecht, S. Winzen, R. Muñoz-Espí, H.P. Schuchmann, K. Landfester, Structure Control in PMMA/Silica Hybrid Nanoparticles by Surface Functionalization, Colloid Polym. Sci. 292 (10) (2014) 2427–2437.
[26] J. Oberdisse, P. Hine, W. Pyckhout-Hintzen, Structure of Interacting Aggregates of Silica Nanoparticles in a Polymer Matrix: Small-Angle Scattering and Reverse Monte Carlo Simulations, Soft Matter 3 (4) (2007) 476–485.
[27] K. Kosugi, H. Arai, Y. Zhou, S. Kawahara, Formation of Organic-Inorganic Nanomatrix Structure with Nanosilica Networks and Its Effect on Properties of Rubber, Polymer 102 (2016) 106–111.
[28] J.L. Keddie, A.F. Routh, Molecular Diffusion Across Particle Boundaries, Springer, Netherlands, 2010, pp. 151–183.
[29] G.W. Scherer, Theory of Drying, J. Am. Ceram. Soc. 73 (1) (1990) 3–14.
[30] A.C. Grillet, S. Brunel, Y. Chevalier, S. Usoni, V. Ansanay-Alex, J. Allemand, Control of the Morphology of Waterborne Nanocomposite Films, Polym. Int. 53 (5) (2004) 569–575.
[31] C.M. Cardinal, Y.D. Jung, K.H. Ahn, L.F. Francis, Drying Regime Maps for Particulate Coatings, AIChE J 56 (11) (2010) 2769–2780.
[32] Y. Li, F. Liu, S. Chen, A. Tsyrenova, K. Miller, E. Olson, R. Mort, D. Palm, C. Xiang, X. Yong, S. Jiang, Self-Stratification of Amphiphilic Janus Particles at Coating Surfaces, Mater. Horiz. 7 (8) (2020) 2047–2055.
[33] A. Fortini, I. Martín-Fabiani, J.L. de La Haye, P-Y. Dugas, M. Lansalot, F. D'Agosto, E. Bourgeat-Lami, J.L. Keddie, R.P. Sear, Dynamic Stratification in Drying Films of Colloidal Mixtures, Phys. Rev. Lett. 116 (11) (2016), 118301.
[34] Y. Tang, G.S. Grest, S. Cheng, Control of Stratification in Drying Particle Suspensions via Temperature Gradients, Langmuir 35 (12) (2019) 4296–4304.
[35] F. Buss, C.C. Roberts, K.S. Crawford, K. Peters, L.F. Francis, Effect of Soluble Polymer Binder on Particle Distribution in a Drying Particulate Coating, J. Colloid Interface Sci. 359 (1) (2011) 112–120.
[36] I. Martín-Fabiani, M.L. Koh, F. Dalmas, K.L. Elidottir, S.J. Hinder, I. Jurewicz, M. Lansalot, E. Bourgeat-Lami, J.L. Keddie, Design of Waterborne Nanoceria/

Polymer Nanocomposite UV-Absorbing Coatings: Pickering versus Blended Particles, ACS Appl. Nano Mater. 1 (8) (2018) 3956–3968.
[37] E. Limousin, I. Rafaniello, T. Schäfer, N. Ballard, J.M. Asua, Linking Film Structure and Mechanical Properties in Nanocomposite Films Formed from Dispersions of Cellulose Nanocrystals and Acrylic Latexes, Langmuir 36 (8) (2020) 2052–2062.
[38] A. Schmid, P. Scherl, S.P. Armes, C.A.P. Leite, F. Galembeck, Synthesis and Characterization of Film-Forming Colloidal Nanocomposite Particles Prepared via Surfactant-Free Aqueous Emulsion Copolymerization, Macromolecules 42 (11) (2009) 3721–3728.
[39] L. Delafresnaye, P.Y. Dugas, P.E. Dufils, I. Chaduc, J. Vinas, M. Lansalot, E. Bourgeat-Lami, Synthesis of Clay-Armored Poly(Vinylidene Chloride-*co*-Methyl Acrylate) Latexes by Pickering Emulsion Polymerization and Their Film-Forming Properties, Polym. Chem. 8 (40) (2017) 6217–6232.
[40] D.K. Makepeace, P. Locatelli, C. Lindsay, J.M. Adams, J.L. Keddie, Colloidal Polymer Composites: Are Nano-Fillers Always Better for Improving Mechanical Properties? J. Colloid Interface Sci. 523 (2018) 45–55.
[41] E. Limousin, N. Ballard, J.M. Asua, The Influence of Particle Morphology on the Structure and Mechanical Properties of Films Cast from Hybrid Latexes, Prog. Org. Coat. 129 (2019) 69–76.
[42] A. Bleier, E. Matijević, Heterocoagulation. Part 3. - Interactions of polyvinyl chloride latex with Ludox Hs silica, J. Chem. Soc., Faraday Trans. 1 74 (0) (1978) 1346.
[43] J.A. Balmer, O.O. Mykhaylyk, J.P.A. Fairclough, A.J. Ryan, S.P. Armes, M. W. Murray, K.A. Murray, N.S.J. Williams, Unexpected Facile Redistribution of Adsorbed Silica Nanoparticles Between Latexes, J. Am. Chem. Soc. 132 (7) (2010) 2166–2168.
[44] S. Li, L.G.J. van der Ven, R.R.M. Joosten, H. Friedrich, R. Tuinier, A.C.C. Esteves, Assembly of Partially Covered Strawberry Supracolloids in Dilute and Concentrate Aqueous Dispersions, J. Colloid Interface Sci. 627 (2022) 827–837.
[45] M.J. Percy, C. Barthet, J.C. Lobb, M.A. Khan, S.F. Lascelles, M. Vamvakaki, S. P. Armes, Synthesis and Characterization of Vinyl Polymer−Silica Colloidal Nanocomposites, Langmuir 16 (17) (2000) 6913–6920.
[46] S.J. Hinder, C. Lowe, J.T. Maxted, J.F. Watts, The Morphology and Topography of Polymer Surfaces and Interfaces Exposed by Ultra-Low-Angle Microtomy, J. Mater. Sci. 40 (2) (2005) 285–293.
[47] J. Crank, The Mathematics of Diffusion, Oxford University Press, 1979.
[48] G.S. Park, Transport Principles - Solution, Diffusion and Permeation in Polymer Membranes, in: P.M. Bungay, H.K. Lonsdale, M.N. Pinho (Eds.), Synthetic Membranes: Science, Engineering and Applications, Springer Netherlands, Dordrecht, 1986, pp. 57–107.
[49] R.A. Gage, E.P.K. Currie, M.A. Cohen Stuart, Adsorption of Nanocolloidal SiO_2 Particles on PEO Brushes, Macromolecules 34 (15) (2001) 5078–5080.
[50] R. Xu, Progress in Nanoparticles Characterization: Sizing and Zeta Potential Measurement, Particuology 6 (2) (2008) 112–115.
[51] R. Minnes, M. Nissinmann, Y. Maizels, G. Gerlitz, A. Katzir, Y. Raichlin, Using Attenuated Total Reflection-Fourier Transform Infra-Red (ATR-FTIR) Spectroscopy to Distinguish between Melanoma Cells with a Different Metastatic Potential, Sci. Rep. 7 (1) (2017) 4381.
[52] M. Schulz, J.L. Keddie, A Critical and Quantitative Review of the Stratification of Particles during the Drying of Colloidal Films, Soft Matter 14 (30) (2018) 6181–6197.
[53] A.F. Routh, W.B. Zimmerman, Distribution of Particles during Solvent Evaporation from Films, Chem. Eng. Sci. 59 (14) (2004) 2961–2968.
[54] H. Luo, C.M. Cardinal, L.E. Scriven, L.F. Francis, Ceramic Nanoparticle/ Monodisperse Latex Coatings, Langmuir 24 (10) (2008) 5552–5561.
[55] R.P. Sear, P.B. Warren, Diffusiophoresis in Nonadsorbing Polymer Solutions: The Asakura-Oosawa Model and Stratification in Drying Films, Phys. Rev. E 96 (6) (2017), 062602.
[56] T. Cosgrove, S.J. Mears, L. Thompson, I. Howell, Adsorption Studies on Mixed Silica -Polymer- Surfactant Systems, in: *Surfactant Adsorption and Surface Solubilization*, 1996, pp. 196–204.
[57] G.P. van der Beek, M.A. Cohen-Stuart, The Hydrodynamic Thickness of Adsorbed Polymer Layers Measured by Dynamic Light Scattering : Effects of Polymer Concentration and Segmental Binding Strength, J. Phys. 49 (8) (1988) 1449–1454.
[58] S. Cheng, G.S. Grest, Dispersing Nanoparticles in a Polymer Film via Solvent Evaporation, ACS Macro Lett. 5 (6) (2016) 694–698.
[59] P.S. Chua, Dynamic Mechanical Analysis Studies of the Interphase, Polym. Compos. 8 (5) (1987) 308–313.
[60] C.G. Robertson, C.J. Lin, M. Rackaitis, C.M. Roland, Influence of Particle Size and Polymer-Filler Coupling on Viscoelastic Glass Transition of Particle-Reinforced Polymers, Macromolecules 41 (7) (2008) 2727–2731.
[61] H.M. Smallwood, Limiting Law of the Reinforcement of Rubber, J. Appl. Phys. 15 (11) (1944) 758–766.
[62] G.P. Baeza, A.C. Genix, C. Degrandcourt, L. Petitjean, J. Gummel, M. Couty, J. Oberdisse, Multiscale Filler Structure in Simplified Industrial Nanocomposite Silica/SBR Systems Studied by SAXS and TEM, Macromolecules 46 (1) (2013) 317–329.
[63] J. Berriot, H. Montes, F. Lequeux, D. Long, P. Sotta, Gradient of Glass Transition Temperature in Filled Elastomers, Europhys. Lett. 64 (1) (2003) 50–56.
[64] Q. Chen, S. Gong, J. Moll, D. Zhao, S.K. Kumar, R.H. Colby, Mechanical Reinforcement of Polymer Nanocomposites from Percolation of a Nanoparticle Network, ACS Macro Lett. 4 (4) (2015) 398–402.
[65] R.P. Kusy, Influence of Particle Size Ratio on the Continuity of Aggregates, J. Appl. Phys. 48 (12) (1977) 5301–5305.
[66] A. Mujtaba, M. Keller, S. Ilisch, H.J. Radusch, T. Thurn-Albrecht, K. Saalwächter, M. Beiner, Mechanical Properties and Cross-Link Density of Styrene-Butadiene Model Composites Containing Fillers with Bimodal Particle Size Distribution, Macromolecules 45 (16) (2012) 6504–6515.
[67] A. Mujtaba, M. Keller, S. Ilisch, H.J. Radusch, M. Beiner, T. Thurn-Albrecht, K. Saalwächter, Detection of Surface-Immobilized Components and Their Role in Viscoelastic Reinforcement of Rubber-Silica Nanocomposites, ACS Macro Lett. 3 (5) (2014) 481–485.
[68] C. Veschambres, M. Halma, E. Bourgeat-Lami, L. Chazeau, F. Dalmas, V. Prevot, Layered Double Hydroxides: Efficient Fillers for Waterborne Nanocomposite Films, Appl. Clay Sci. 130 (2016) 55–61.
[69] I. Martín-Fabiani, J. Lesage de la Haye, M. Schulz, Y. Liu, M. Lee, B. Duffy, F. D'Agosto, M. Lansalot, J.L. Keddie, Enhanced Water Barrier Properties of Surfactant-Free Polymer Films Obtained by MacroRAFT-Mediated Emulsion Polymerization, ACS Appl. Mater. Interfaces 10 (13) (2018) 11221–11232.
[70] M. Khalfaoui, S. Knani, M.A. Hachicha, L.A. Ben, New Theoretical Expressions for the Five Adsorption Type Isotherms Classified by BET Based on Statistical Physics Treatment, J. Colloid Interface Sci. 263 (2) (2003) 350–356.
[71] R.M. Felder, G.S. Huvard, 17. Permeation, Diffusion, and Sorption of Gases and Vapors, in: Methods in Experimental Physics, Vol. 16, Academic Press, 1980, pp. 315–377.
[72] J. Liao, C. Zhu, B. Gao, Z. Zhao, X. Liu, L. Tian, Y. Zeng, X. Zhou, Z. Xie, Z. Gu, Multiresponsive Elastic Colloidal Crystals for Reversible Structural Color Patterns, Adv. Funct. Mater. 29 (39) (2019) 1902954.